Raman spectra of silicon carbide small particles and nanowires

2005 J. Phys.: Condens. Matter 17 2387

(http://iopscience.iop.org/0953-8984/17/15/010)

INSTITUTE OF PHYSICS PUBLISHING JOURNAL OF PHYSICS: CONDENSED MATTER

J. Phys.: Condens. Matter **17** (2005) 2387–2395 doi:10.1088/0953-8984/17/15/010

Raman spectra of silicon carbide small particles and nanowires

Monika Wieligor, Yuejian Wang and T W Zerda[1]

TCU, Department of Physics and Astronomy, Fort Worth, TX 76120, USA

E-mail: t.zerda@tcu.edu

Received 17 January 2005, in final form 3 March 2005
Published 1 April 2005
Online at stacks.iop.org/JPhysCM/17/2387

Abstract

Two manufacturing protocols of silicon carbide (SiC) nanowires are discussed. The Raman spectra of produced SiC nanowires are compared with spectra of SiC powders of various grain sizes. The temperature and pressure dependence of the Raman spectra for powders is similar to that of bulk crystals, but is different for nanowires. Frequency shifts, band broadenings and the presence of shoulders are discussed in terms of crystal size, character of defects and their population. The concentration of defects in synthesized nanowires depends on the sintering method. Raman intensity enhancement of the LO phonon was observed when the wavelength of the excitation laser was changed from 780 to 514 nm.

1. Introduction

Silicon carbide (SiC) is a wide-gap semiconductor with many superb properties, such as high hardness, high thermal conductivity, low coefficient of thermal expansion, and excellent resistance to erosion and corrosion [1, 2]. It also exhibits interesting electronic and optical properties, which vary with the size of particles. The relationship between grain size and material properties has been studied for a large number of materials [3–6], including SiC [7–11]. Recently SiC nanowires (NWs) have been produced and although their mechanical properties are very promising [8, 12–14] little is known about their microstructure and electronic/optical properties. SiC nanowires have been obtained by various methods, including carbothermal reduction of Si and carbon nanotubes [15], chemical vapour deposition [16, 17], reaction between $SiCl_4$ and CCl_4 with sodium as co-reductant [18], carbon nanotube-confined reaction [19, 20], and annealing carbon nanotubes covered with Si [21]. These methods either require high temperature for vapour–vapour [15] or solid–vapour [19, 20] reactions, or need a metal catalyst, Fe, Cu, or Ni, [16, 17]. In this study, we present an alternative synthesis of SiC nanowires that does not require catalysts or very high temperatures.

[1] Author to whom any correspondence should be addressed.

0953-8984/05/152387+09$30.00

The first detailed description of Raman spectra of bulk SiC is due to Olego and Cardona [22, 23], who assigned all detectable peaks to corresponding phonon modes. To the best of our knowledge no dedicated Raman study on nanosize effects in SiC has been published. Raman spectra of various nanosize materials have been successfully applied to understand their structure and morphology [4, 8, 25]. For example, Nemanich *et al* [4] observed asymmetric broadening of Raman lines and frequency shifts when the crystal size was decreasing. They explained these effects in terms of the phonon confinement model.

In this paper we report Raman spectra of SiC nanowires of two different mean diameters, 20 nm (sample NW-A) and 200 nm (sample NW-B), and lengths approaching several hundred microns, and contrast them with spectra obtained for commercial powders of average grain sizes varying between 20 and 400 nm. All specimens were β-SiC and no traces of α-SiC were detected by x-ray powder diffraction measurements. Temperature and pressure effects on peaks position and broadening are discussed and results used to evaluate the microstructure and properties of nanowires.

2. Experimental details

β-SiC powders of average grain sizes 20, 50, 220 and 400 nm were purchased from Aldrich (Milwaukee, Wisconsin) and Nanostructured & Amorphous Materials Inc (Los Alamos, New Mexico). β-SiC nanowires were prepared in our laboratory from multiwall carbon nanotubes (MWNTs) (outer diameter: 60–100 nm) and nanosize Si powder (grain size: $<$100 nm). The molar ratio of starting materials was 1:3.5. The MWNTs were purchased from Nanostructured &Amorphous Materials Inc (Los Alamos, New Mexico) and Si powder from Aldrich (Milwaukee, Wisconsin).

To make uniform mixtures both powders were dispersed in absolute ethyl alcohol using an ultrasonic processor. After drying, the mixtures were compressed into solid tablets at 200 bar for several minutes. The tablets were placed in the middle of a graphite cylinder and closed by two graphite disks. Next, the tablets were sintered for one hour in a conventional furnace, at 1250 °C in the case of NW-A and at 1450 °C for NW-B. Before and during heat treatment the furnace was purged with argon. A graphite cylinder and graphite caps were used to prevent oxidation of MWNTs during sintering. Indeed, test runs at the same experimental conditions with only pure MWNTs showed no mass losses and no oxidation. After heating, the synthesized samples contained silicon carbide, unreacted silicon, and MWNTs. To remove the remaining MWNTs and Si, the specimens were heat treated in air at 800 °C and then treated with hot dilute KOH and washed in absolute alcohol and distilled water. No traces of Si were found by x-ray diffraction (XRD) or Raman spectroscopy in the cleaned specimens; see figure 1. The nanowire morphology was confirmed by transmission electron microscopy (TEM); see figure 2.

X-ray diffraction patterns were measured with a PW2773 (Philips, Japan) diffractometer with Cu Kα radiation ($\lambda = 1.540\,56$ Å), operated at 35 kV and 30 mA. The measurement range of 2Θ was from 20° to 150° with a step of 0.02° and an exposure time of 3 s.

Raman spectra were obtained using a Raman microimaging system containing an argon-ion laser, an Olympus BH-2 microscope, a Kaiser dispersive spectrometer and a front illuminated CCD detector from Roper. The laser operated at 514 nm and its power at the sample varied from 0.01 to 0.15 W. Selected experiments were repeated using a 780 nm laser. Spectral resolution was about 4.0 cm^{-1}. The objective, 40×, allowed collecting scattered light from spots as small as 1.5 μm in diameter. The spectra were obtained with exposure time varying between 30 s and 2.5 min, and were analysed using GRAMS software. In general, spectra were curve fitted using Lorentzian–Gaussian functions to determine the exact positions of the Raman bands.

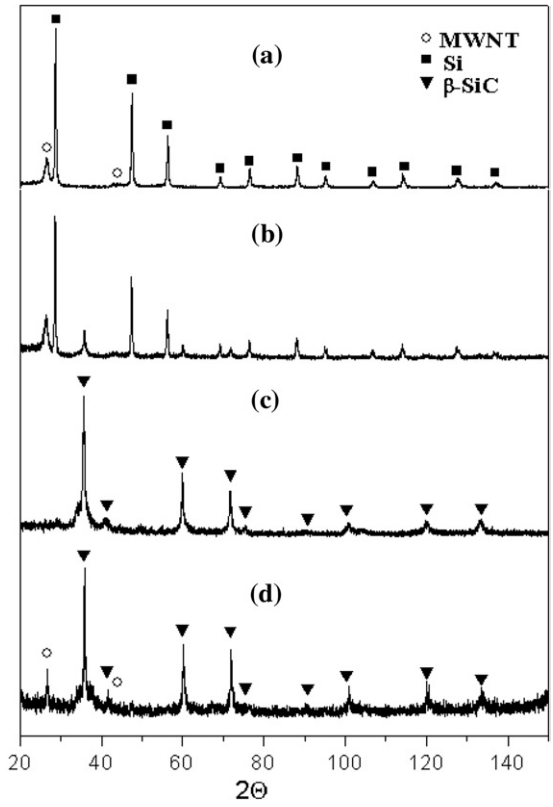

Figure 1. (a) XRD of the initial mixture; (b) after sintering at 1200 °C; (c) sample NW-A after thermal treatment which removed unreacted silicon and carbon nanotubes, (d) sample NW-B after oxidation and chemical treatment which removed silicon and some carbon nanotubes.

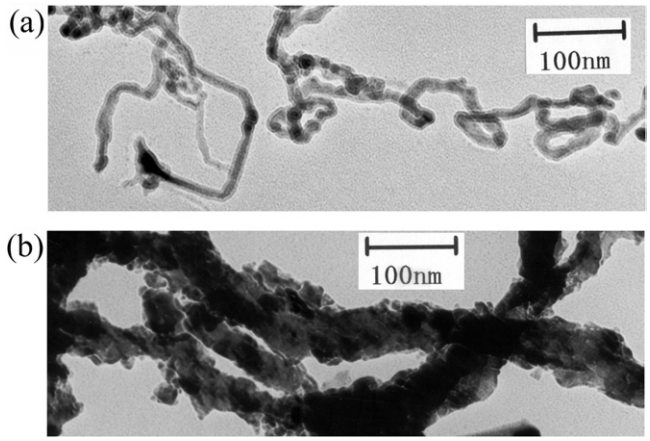

Figure 2. Typical TEM images of SiC nanowires: (a) NW-A, sintered at 1200 °C, (b) NW-B, sintered at 1450 °C.

High-pressure measurements were carried out at room temperature using a 514 nm laser in a gasketed diamond anvil cell. The force applied on the opposing diamond anvils was

transmitted via an alcohol to the sample and the diamond anvils served as the optical windows through which Raman scattering was excited and collected. The pressure chamber was defined by the volume of a 156 μm diameter hole drilled at the centre of the diamond indentation in a hardened stainless steel gasket. A small amount of SiC crystallites with a tiny ruby chip as a pressure sensor were placed inside the gasket hole which was then filled with methanol–ethanol (4:1 volume ratio) mixture. The pressure was calibrated to within 2% using the standard ruby R-line emission.

3. Results

X-ray diffraction spectra of NW-A showed only peaks characteristic for SiC with cubic symmetry (3C or β phase), see figure 1(c), while that of NW-B in addition to SiC peaks also showed peaks due to MWNTs, figure 1(d). The peaks due to the carbon nanotubes were not removed even by long oxidation at 800 °C. Peaks characteristic for MWNTs were present in the Raman spectra of NW-B but absent in the spectra of NW-A. Typical TEM images of the initial mixture showed twisted and interweaved carbon nanotubes. In figure 2(a), sample NW-A, SiC in the form of threads of thickness mostly close to 20 nm in diameter can be observed. Often one or both ends of threads were attached to large grains of silicon carbide. TEM images of NW-B, figure 2(b), showed thread-like structures of diameters similar to the diameters of the MWNT precursor. Combining the x-ray and TEM results we concluded that in specimen B SiC was present on the surface and carbon nanotubes constituted the interior. The SiC layer coated the carbon nanotubes and effectively isolated the carbon atoms from oxygen, and thus prevented oxidation of the MWNTs during high temperature treatment in air.

SiC has main Raman peaks centred at 796 and 973 cm^{-1} which correspond to the transverse optic (TO) and longitudinal optic (LO) modes, respectively [22]. The dominant role of the carbon atom in the dynamics of 3C-SiC is expressed by the behaviour of the phonon dispersion curves, which are more similar to those of diamond than to those of silicon [26]. But the selection rules for diamond and zinc-blende structures (3C-SiC) are different. For example, in diamond, the TO and LO modes are triply degenerate at the centre of the Brillouin zone [3]. In contrast the LO and TO modes for 3C-SiC are split at the Γ point because of the polar character of SiC. The weak dispersion of the LO and TO phonon branches causes the gap and pronounced maxima in the optical range of the one-phonon density of states of 3C-SiC [26, 27]. The LO band has its intensity dependent on the wavelength of the incident laser. Close to the resonance, when the 514 nm laser excitation line carrying energy close to that of the band gap energy of 2.4 eV was used, the LO band had its intensity similar to that of the TO band, but when the 780 nm laser was used, the LO band had intensity much smaller than the TO peak; see figure 3(a). For sample NW-B, figure 3(b), the TO and LO bands were clearly seen as two strong peaks when the 514 nm excitation wavelength was used, but for the 780 nm laser two very broad peaks centred at about 915 and 860 cm^{-1} dominated in the spectral region between 800 and 1000 cm^{-1}.

Silicon carbide is a material that effectively absorbs light, including the incident laser light. During this process the sample's temperature increases and this may cause frequency shifts. This effect may overlap with shifts due to other effects and must be separated. For this reason we decided to study the effect of temperature on SiC spectra carefully. Raman spectra for SiC were recorded at temperatures between room temperature and 450 °C. To reduce laser induced heating effects, during these studies we applied a very small laser power of 0.01 W, and to collect spectra of high signal to noise ratio we used long exposure times. The peak positions were determined for the LO and TO phonons and plotted as a function of temperature. A softening of the phonon frequencies with increasing temperature was observed for both modes and was

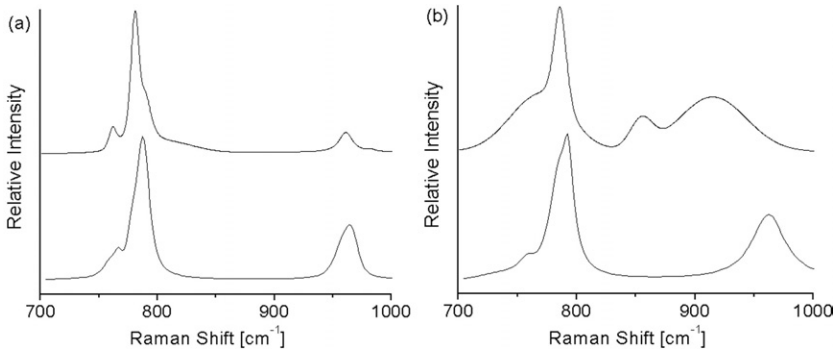

Figure 3. Typical Raman spectra in the 700–1000 cm^{-1} region collected using 514 nm laser (bottom curve) and 780 nm excitation wavelength (top curve): (a) SiC powder of average grain size 220 nm, (b) specimen NW-B.

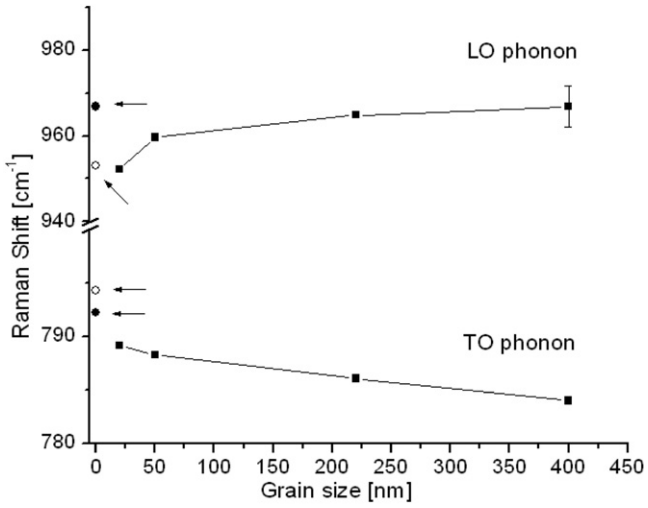

Figure 4. Frequencies of the TO and LO phonons for SiC as a function of grain size. The solid lines are shown to guide the eye.

approximated by linear functions. These functions were used to estimate the temperature of SiC at the laser focus in subsequent studies.

During the experiments we observed that with decreasing grain size the intensity of the Raman lines of SiC was decreasing, the LO and TO peaks became increasingly broader and asymmetric, and their frequency shifted. Figure 4 shows the positions of TO and LO peaks as a function of grain size. For comparison purposes, in that figure we also indicate the positions of the phonon bands of NW samples. Open circles indicate values obtained for NW-A, 794 cm^{-1} (TO) and 953 cm^{-1} (LO), and full circles those for NW-B, 792 cm^{-1} (TO) and 964 cm^{-1} (LO). These measurements were conducted at a very low laser power, 0.05 W, and we estimate that the temperature at the laser focus increased only to a negligible small value of $150 \pm 50\,^{\circ}C$. It is seen that with a decrease of the grain size the TO phonon shifts to higher energy, and the LO phonon to lower energy.

For small size crystals the TO peak is accompanied by a shoulder on the low frequency side. For SiC of average grain sizes of 400 and 220 nm the shoulder was observed at 765.5 cm^{-1}.

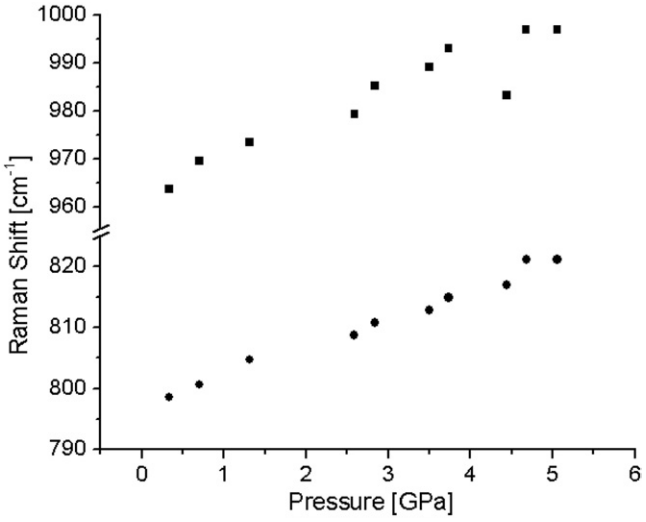

Figure 5. Pressure dependence of the TO (circles) and LO (squares) phonons for NW-B. The spectra were obtained with the 514 nm laser.

For 20 nm crystals it was observed at 761.5 cm^{-1} and for NW-B at 757 cm^{-1}. In the case of NW-A we obtained Raman spectra that varied with position of the incident laser on this sample surface. The centres of the TO line and the shoulder varied between 790 to 794 cm^{-1} and 757 to 769.5 cm^{-1}, respectively. Recently, Rohmfeld *et al* [28] showed that the separation between the TO peak and the shoulder reflects the average distance between stacking faults. Since this value for NW-A varied widely we concluded that the structure of specimen A was not uniform.

The hydrostatic pressure dependence of the TO and LO phonons frequencies of bulk SiC was investigated by Olego and Cardona [22, 23]. They observed that with increasing pressure these frequencies shifted toward higher values. Our studies for nanosize SiC powders and nanowires conducted at room temperature and pressures up to 50 kbar (5 GPa) confirmed these results; see figure 5. As expected, we did not observe any indication of a possible phase transition. With increasing pressure the peaks significantly broaden and the peak maxima shift.

4. Discussion

The LO and TO Raman bands of SiC change their shapes with temperature, pressure, crystal size, defects character and concentration. In silicon carbide twins, dislocations, and inclusions have been observed, but the most common defects are stacking faults [29]. The size dependence of band position has been observed for many materials and is often used to evaluate crystal size [4, 30]. This effect can be explained in terms of the phonon confinement model [4, 13, 14]. For an infinite crystal only vibrations from the centre of the Brillouin zone can be active in the first-order Raman scattering. A short range disorder, bond distortion or nanocrystallinity can destroy periodicity and confine the phonon spatially. This introduces an uncertainty on the reduced vector in the Brillouin zone. In crystals of finite sizes a relaxation of Raman transition rules allows for transitions with $\Delta k \neq 0$, and when the phonon dispersion curves inside the first Brillouin zone are not flat it results in band shift and broadening. The TO phonon distribution curve for SiC shows very little dispersion within the first zone, and although

transitions other than those close to the zone centre are allowed, they all have similar frequencies and consequently do not lead to a shift of the peak. Thus, the TO band position dependence on crystal size, see figure 4, is not caused only by the space confinement and must be attributed to other effects. We can exclude a variation of temperature as a source of the shift, as all experiments were conducted for the same surface temperature of about 150 °C. The presence of defects is the most likely explanation for the observed frequency shifts.

The LO band shifts toward lower frequencies when the selection rules are relaxed and transitions other than for $\Delta k = 0$ are allowed. Such behaviour was predicted by the shape of the phonon dispersion curve, which decreases steeply in every direction from the zone centre. However, in view of the discussion of the TO band position dependence on effects other than the crystal size, it is reasonable to assume that the LO band is also affected by the presence of defects, strains and surface layer, and the observed frequency shift cannot be used to evaluate grain sizes.

The existence of defects is also manifested by large band widths and the presence of shoulders. Based on the assumption that the position of the TO shoulder is a measure of concentration of stacking faults, we evaluated that the highest concentration of stacking faults was in NW-B. We also concluded that the population of stacking faults in specimen A was very high, but in contrast to sample B it varied from one location within the sample to another. This conclusion is based on the fact that the shoulder's position relative to the TO centre was different for various points on the surface of NW-A, and varied between 24 and 33 cm^{-1}. The origin of the different distribution of stacking faults within NW-A is in its manufacturing protocol. This sample was obtained at a relatively low temperature, below the melting point of silicon. The SiC nanowires obtained had diameters of about 20 nm and often exceeded lengths of 500 nm. TEM images show straight nanowires along with twisted and entangled threads of similar diameter. In such diverse structures abundant stacking faults of non-uniform distribution could exist.

At 1450 °C, the temperature used to manufacture NW-B, nanosize silicon melts, and it is reasonable to assume that it completely covers the outside surface of the carbon nanotubes. TEM images indicate that the sample consists of a core in the form of a carbon nanotube coated with nanosize SiC in the form of tiles. These tiles have different shapes, sizes, and orientations and partially overlap. Such a morphology is expected for a product of a reaction with a significant number of nuclei; in the case of carbon nanotubes these are probably defect sites. The formation of nanocrystalline SiC originated on the surface of carbon nanotubes at these sites. Once nanocrystallites covered the outer surface of the carbon nanotubes, the reaction rate was limited by the diffusion rate of carbon atoms from MWNTs through SiC toward silicon, or silicon atoms towards the nanotubes. It is reasonable to assume that diffusion paths through grains require higher activation energy than paths through grain boundaries. Such a mechanism would facilitate tile-like growth of SiC.

At a first glance the diameter of an NW could be considered a measure of the size of the grains. Applying the Scherrer method to x-ray diffraction spectra of NW-B we obtained 30 nm for the size of crystallites, in good agreement with the dimensions of the tiles estimated from the TEM images in figure 2(b). This result indicates that the SiC tiles were composed of crystallites whose boundaries were defined by defects. Even better agreement was obtained for NW-A. The average size of crystallites estimated from the (111) reflection was 20 nm.

The broad band centred at about 860 cm^{-1} has been observed previously in nanosize SiC by Zhang *et al* [14], who assigned it to Frohlich transitions enhanced by structure defects. We observed this structure only with the 780 nm laser, and its intensity appears to be correlated with the crystal size and the population of defects. For the 400 nm grains it is barely noticeable, for 50 nm grains and NW-B its intensity is moderately increased, but for NW-A its intensity

is comparable with the TO peaks. The origin of the 915 cm^{-1} peak remains unknown; we speculate, however, that its intensity is also related to structure defects.

As the pressure is increased the separation between the TO and LO peaks increases. The data for 220 nm particles practically matched the high pressure data obtained in [22–24] for bulk SiC. These authors explained the pressure induced shift in ω_{LO}^2–ω_{TO}^2 in terms of increasing transverse effective charge:

$$\omega_{LO}^2 - \omega_{TO}^2 = \frac{4\pi N e^{*2}}{M\varepsilon_\infty}$$

where M is the reduced mass of the ions, ε_∞ is the optical dielectric constant, N is the number of atoms in an unit volume, and e^* is the transverse charge. For small particles the number of atoms close to the surface is comparable to that in the interior of the particle. The core-shell model of nanosize crystals assumes that in the core atoms are arranged in the crystallographic structure identical to that of bulk crystal, but the outer layers of the nanocrystals, the shells, although also arranged in the same crystallographic structure, have interatomic distances that are slightly increased (SiC, diamond) or decreased (GaN) [7, 31]. The effective charge could thus be separated into two components, one arising from the polarization in the core and the other from the outer layer [9]. The surface atoms may contribute less to the polarization than the core atoms because of the lack of counter-ions outside the grain. In addition, the different arrangement of this layer may further reduce the contribution to the overall polarization and thus reduce the value of the effective charge. Thus, the core-shell model may explain a smaller splitting noted for grains of smaller size, including the smaller splitting observed for NW-A than for NW-B. The crystallites in NW-B are slightly larger than those in NW-A.

For both NW-A and NW-B, the splitting increases rapidly with increasing pressure and approaches the value observed for bulk SiC. Apparently, the structure of the surface layer is altered by increased pressure. Indeed, high pressure x-ray diffraction measurements conducted for nanosize SiC powder indicated that the surface layer had an expanded structure with lattice constant slightly larger than that for the bulk crystal [7]. But as the pressure was increased the lattice constant of the surface layer decreased at a faster rate than that of the interior, and there was practically no difference in lattice parameters of the surface layer and the core [7]. A more rapid compression of outer layers for nanowires explains the large splitting between the LO and TO bands at low pressures. But when the compressions of both the surface layer and the core were similar the splitting approached the value observed for bulk material.

Stacking faults are the most common defects in bulk SiC. The frequency separation between the TO peak and its shoulder can be used to estimate their concentration. As the pressure increased to 5 GPa, this separation decreased by 10 wavenumbers, indicating that the population of stacking faults was reduced. It is interesting to note that the reduction in the distance between the TO band and the shoulder was not affected by the release of pressure. This pressure induced annealing of NW-B was permanent. No such effect was observed for NW-A.

5. Conclusion

SiC nanowires with two different mean diameters, 20 and 200 nm, and lengths approaching several hundred microns were obtained by reaction between MWNTs and silicon in the liquid phase at 1450 °C (NW-B) and in the solid phase at 1250 °C (NW-A). NW-B had the core in the form of carbon nanotubes completely covered by nanosize SiC in the form of tiles. In both specimens the concentration of defects, especially stacking faults, was very high, as indicated by the frequency separation between the TO peak and its low frequency shoulder,

large bandwidths of phonon peaks, and the enhanced intensity of the defect sensitive band at about 860 cm^{-1}. In NW-A synthesized at 1250 °C, the concentration of defects was not uniform and varied within the sample from one location to another.

There was no correlation between the frequencies of SiC phonons and grain sizes. The pressure dependence of the frequency splitting between the TO and LO phonons was explained in terms of the core-shell model of nanosize crystallites. Pressure treatment reduced the population of defects in the nanowires.

References

[1] Choyke W J and Pensl G 1997 *Mater. Res. Bull.* **22** 25
[2] Nakashima S and Harima H 1997 *Phys. Status Solidi* a **162** 39
[3] Martin T P and Genzel L 1973 *Phys. Rev.* B **8** 1360
[4] Nemanich R J, Solin S A and Martin R M 1981 *Phys. Rev.* B **23** 6348
[5] Silvestri M R and Schroeder J 1995 *J. Phys.: Condens. Matter* **7** 8519
[6] Qadri S B, Yang J, Ratna B R, Skelton E F and Hu J Z 1996 *Appl. Phys. Lett.* **69** 2205
[7] Palosz B, Grzanka E, Stel'makh S, Gierlotka S, Pielaszek R, Bismayer U, Weber H-P, Proffen Th and Palosz W 2003 *Solid State Phenom.* **94** 203
[8] Yan Y, Zhang S L, Fan S, Han W, Meng G and Zhang L 2003 *Solid State Commun.* **126** 649
[9] Sasaki Y, Nishina Y, Sato M and Okamura K 1989 *Phys. Rev.* B **40** 1762
[10] Collins A K, Pickering M A and Taylor R L 1990 *J. Appl. Phys.* **68** 6510
[11] Bind J-M and Biggers J V 1976 *J. Appl. Phys.* **47** 5171
[12] Quadri S B, Imam M A, Feng C R, Rath B B, Yousuf M and Singh S K 2003 *Appl. Phys. Lett.* **83** 548
[13] Shi W, Zheng Y, Peng H, Wang N, Lee C, Lee S-T and Petrovic J J 2000 *J. Am. Ceram. Soc.* **83** 3228
[14] Zhang S-L, Zhu B-F, Huang F, Yan Y, Shang E, Fan S and Han W 1999 *Solid State Commun.* **111** 647
[15] Gao Y H, Bando Y, Kurashima K and Sato T 2001 *Scr. Mater.* **44** 1941
[16] Zhou X T, Wang N, Lai H L, Peng H Y, Bello I, Wong N B, Lee C S and Lee S T 1999 *Appl. Phys. Lett.* **74** 3942
[17] Lai H L, Wong N B, Zhou X T, Peng H Y, Frederic C K Au, Wang N, Bello I, Lee C S, Lee S T and Duan X F 2000 *Appl. Phys. Lett.* **76** 294
[18] Lu Q, Hu J, Tang K, Qian Y, Zhou G, Liu X and Zhu J 1999 *Appl. Phys. Lett.* **75** 507
[19] Dai H, Wong E W, Lu Y, Fan S and Liber C M 1995 *Nature* **375** 769
[20] Han W, Fan S, Li Q, Liang W, Gu B and Yu D 1997 *Chem. Phys. Lett.* **265** 374
[21] Liu J, Zhong D, Xie F, Sun M, Wang E and Liu W 2001 *Chem. Phys. Lett.* **348** 357
[22] Olego D and Cardona M 1982 *Phys. Rev.* B **25** 1151
[23] Olego D and Cardona M 1982 *Phys. Rev.* B **25** 3878
[24] Debernardi A, Ulrich C, Syassen K and Cardona M 1999 *Phys. Rev.* B **59** 6774
[25] Ward Y, Young R J and Shatwell R A 2001 *J. Mater. Sci.* **36** 55
[26] Karch K, Pavone P, Windl W, Shütt O and Strauch D 1994 *Phys. Rev.* B **50** 17054
[27] Feng Z C, Mascarenhas A J, Choyke W J and Powell A 1988 *J. Appl. Phys.* **64** 3176
[28] Rohmfeld S, Hundhausen M and Ley L 1998 *Phys. Rev.* B **58** 9858
[29] Vetter W M and Dudley M 2004 *J. Cryst. Growth* **260** 201
[30] Li B, Yu D and Zhang S L 1999 *Phys. Rev.* B **59** 1645
[31] Palosz B, Grzanka E, Pantea C, Zerda T W, Wang Y, Gubicza J and Ungar T 2005 *J. Appl. Phys.* at press